Research Article

Mechanism and Optimized Process Conditions of Forming One-Dimensional ZnO Nanorods with Al-Doping by Electrodeposition Method

Jianlin Chen ,[1,2] **Yu Zhang,**[1,2] **Wei Qiu,**[1,2] **Shu Chen,**[1,2] **Chang Liu,**[1,2] **Zhuoyin Peng,**[1,2] **and Jian Chen** [1,2]

[1]*School of Energy and Power Engineering, Changsha University of Science & Technology, Hunan 410114, China*
[2]*Key Laboratory of Energy Efficiency and Clean Utilization, Education Department of Hunan Province, Changsha University of Science & Technology, Hunan 410114, China*

Correspondence should be addressed to Jian Chen; chenjian_513@126.com

Textured transparent conductive electrodes for thin-film solar cells have been considered as an effective route for enhancing sunlight harvest due to light trapping. Here, we report a self-assembling electrochemical approach for preparing Al-doped ZnO nanorod arrays (NRAs) as light-trapping electrodes from a mixed aqueous solution of zinc nitrate and aluminium nitrate. The mechanism and optimized process conditions of forming one-dimensional ZnO nanorods with Al-doping were systematically investigated. The results showed that Al atoms were successfully doped into ZnO crystal lattice, and the morphologies could be controlled by adjusting the Al^{3+}/Zn^{2+} ratio in the precursors and deposition time. The Al-doped ZnO films grew into well-aligned hexagonal NRAs with c-axis perpendicular to the substrates and then transited into a mixture of nanosheets and nanorods with Al^{3+}/Zn^{2+} ratio increasing. They exhibited good electrical conductivity with a sheet resistance of 68-167Ω/square and appropriate visible light transmittance of 61-82%. Taking into account of desired morphology and phase purity, as well as good electrical conductivity and optical transmittance, the optimal window of Al^{3+}/Zn^{2+} ratio in the precursors was determined between 1 at% and 2 at% with applied potential of -1.5V, bath temperature of 80°C, and deposition time of about 30min. The electrodeposition method provides a facile and efficient route for obtaining large-area textured transparent electrodes at a low cost.

1. Introduction

The hexagonal wurtzite zinc oxide (ZnO) is a direct wide band gap semiconductor (~3.37 eV) with a relatively high exciton binding energy (~60 meV) at room temperature [1]. Due to its many excellent characteristics, it promises diverse applications, such as short-wavelength light-emitting diodes and lasing devices [2], transparent conductive oxide (TCO) films [3], piezoelectric transducers [4, 5], ultraviolet photodetectors [6], diluted magnetic semiconductors [7], gas sensors [8, 9], dye-sensitized solar cells [10–14], organic and polymer solar cell's electron transport layers [15, 16], photo-

catalytic degradation and hydrogen production [17–24]. Also, n-type doped (e.g., Al, Ga, or In-doped) ZnO films have been extensively used as transparent electrodes of thin-film solar cells due to their superior advantages, such as high optical transparency, excellent electrical conductivity, high stability in hydrogen plasma atmosphere, nontoxicity, inexpensive and abundant raw materials, and diversity of fabrication methods [25, 26]. ZnO has also attracted great interest due to its unique ability to form a variety of one-dimensional nanostructures [27]. Over the past decades, various methods have been developed to fabricate complex and oriented ZnO nanostructure arrays, including chemical

vapor deposition, vapor-liquid-solid, sol-gel, hydrothermal, spray pyrolysis, and electrodeposition methods. In comparison with other methods, the electrodeposition method represents a facile route for synthesizing a well-aligned ZnO nanowire [28, 29], nanorod [30], or nanotube arrays [31] on transparent conductive oxide substrates. It is convenient to tune the crystal shape, diameter, length, aspect ratio, morphology, orientation, and distribution by adjusting the growth parameters including applied potential, ion concentration, pH value, temperature, deposition time, seeded substrates, and active agents [32–34]. So far, intrinsic ZnO one-dimensional nanostructures have been intensively studied for light-trapping or electron transport structures for diverse solar cells [35–44]. On the contrary, there are very few studies focusing on foreign atom being doped into ZnO nanostructures via the electrosynthesis process [45, 46].

However, the electrical conductivity of intrinsic ZnO nanostructures is limited due to low carrier concentration, which will greatly increase the series resistance of solar cells to degrade the photovoltaic performance. It is well known that the group III atoms, such as B, Al, Ga, and In, being doped into ZnO can greatly increase the carrier concentration and thus the conductivity, which is related to the contribution from group III atom substituting Zn site leading to one extra free electron. Also, previous studies have shown that the electron transport velocity along the c-axis of one-dimensional ZnO crystals was several orders of magnitude faster than that of randomly preferred crystalline ZnO particles [10]. Both of these may enhance the conductivity of group III-doped well-aligned ZnO nanorod arrays (NRAs). In addition, the size of ZnO nanorods is comparable to the visible light wavelengths of the solar spectrum, which facilitates their unique light scattering and capturing effects. In view of these factors, transparent conductive group III-doped ZnO NRAs may be used as transparent electrodes for thin film-based solar cells, such as a-Si, dye-sensitized or quantum dot-sensitized, copper indium gallium selenide (CIGS), and perovskite solar cells. The one-dimensional nanostructures with proper geometrical configuration not only can trap photons more effectively but also facilitate collecting the photo-induced electrons, both of these leading to enhancement of power conversion efficiency. Furthermore, the increasing contacting area between transparent conductive ZnO NRA electrodes and active layers of thin-film solar cells will do benefit to collecting photo-induced electrons more efficiently and quickly, reducing charge accumulation at the interfaces. Nevertheless, the approaches of doping group III atoms into one-dimensional ZnO single crystallize arrays at large-area and low cost still remain a significant challenge. The mechanism of doped ZnO nanostructures from a zinc nitrate aqueous solution with doping ions has not been thoroughly clarified, which is vital for well tuning the morphology and foreign atoms being effectively doped into ZnO lattice.

In this work, in order to obtain transparent conductive ZnO with light-trapping effect, the electrosynthesis mechanism and process of Al-doped ZnO NRAs on fluorine-doped tin oxide (FTO) glass substrates from a mixed aqueous solution of zinc nitrate and aluminium nitrate with different Al^{3+}/Zn^{2+} ratio were systematically investigated.

2. Materials and Methods

Zinc nitrate hexahydrate $[Zn(NO_3)_2 \bullet 6H_2O]$ and aluminium nitrate nonahydrate $[Al(NO_3)_3 \bullet 9H_2O]$ with analytical reagent grade were the starting materials of Zn and Al, respectively. The samples were grown by electrodeposition method from zinc nitrate and aluminium nitrate mixed aqueous solutions without other auxiliary reagents on FTO film glass substrates with a sheet resistance of 15-18Ω/sq at an applied potential of -1.5V. All electrodepositions were carried out potentiostatically at 80°C in a two-electrode system with a FTO conductive glass piece as the working-electrode and a platinum-titanium composite mesh as the counter electrode. The distance between the working electrode and the counter electrode was kept 2cm. The concentration of zinc nitrate in the solutions was 3mmol/L, and the amount of aluminium nitrate nonahydrate was added according to different Al^{3+}/Zn^{2+} ratio of 0, 1, 2, and 3 at % in the precursors. Prior to each electrodeposition run, the FTO substrates were ultrasonically cleaned in acetone and ethanol for 30min in each solvent, respectively. At the end of the growth period, the FTO substrates covered with ZnO were removed from the solution and immediately rinsed in flowing deionized water to eliminate any residual impurities from the surface. Finally, the samples were thermally treated at 530°C in air for 1h and 420°C in a vacuum for 30min in sequence.

The crystallographic characterization was investigated by an X-ray diffractometer (XRD, D/Max-rA, Japan). The micrograph and chemical composition were observed by field emission scanning electron micrographs (FESEM, JSM-6700F, Japan) with an energy dispersive X-ray spectrometer (EDS). Transmission electron microscopy (TEM) images were obtained on a microscope (Tecnai G^2 F20 S-TWIN, USA) with an accelerating voltage of 200 kV. The X-ray photoelectron spectroscopy (XPS) measurement was performed to confirm the element status of samples on an ultrahigh-vacuum electron spectrometer (VG ESCALAB 250Xi, USA). The sheet resistance was measured by an M-3 four-probe tester (Suzhou Jingge Electronic Co. Ltd, China). The cyclic voltammogram spectrum test was carried out using a German Zahner electrochemical workstation.

3. Results and Discussion

3.1. Reaction and Growth Mechanism. As many previous reports depicted, a fundamental reaction in electrodepositing ZnO from the $Zn(NO_3)_2$ aqueous solutions is based on the reduction of nitrate ions into nitrite ions with OH⁻ ions generating [47]. The ZnO formation is not a simple faradaic process but an electrochemically induced precipitation process. The local OH⁻ ion concentration increase will lead to the reversible precipitating reaction of OH⁻ and Zn^{2+} ions. Then, the formed $Zn(OH)_2$ is transformed into ZnO at elevated temperature. If there are some Al^{3+} ions also existing in the solutions, similar reactions may

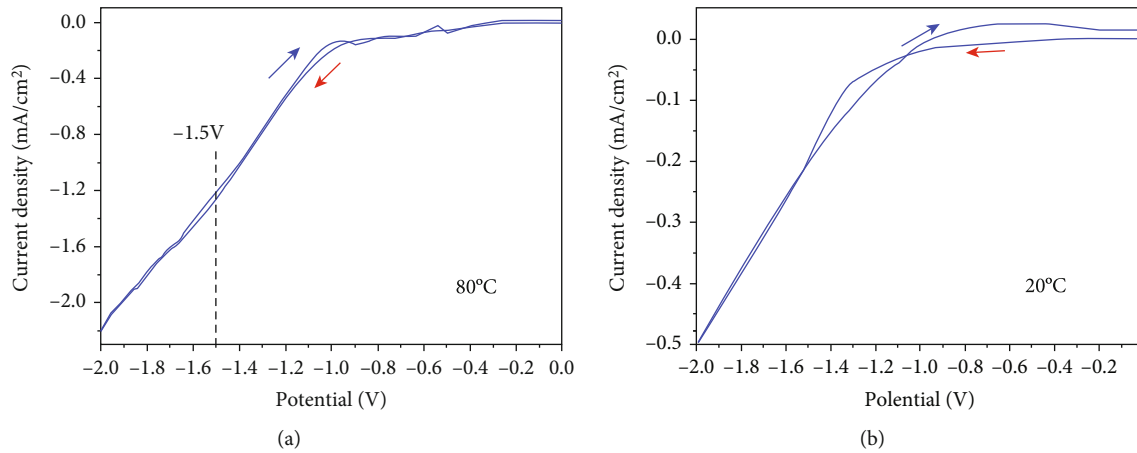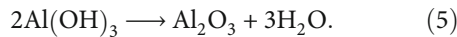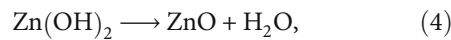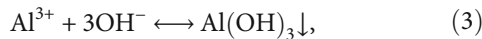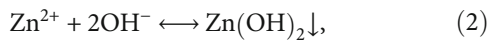FIGURE 1: Cyclic voltammogram of the 3 mM $Zn(NO_3)_2$ aqueous solutions on FTO-coated glass with the working and counter electrode distance 2 cm and the scan rate 30 mV/s at (a) 80°C and (b) 20°C.

occur. The doping mechanism is believed to be coprecipitation of $Zn(OH)_2$ with Al^{3+} substituting Zn^{2+} sites [48]. The reactions can be generally listed as follows:

$$NO_3^- + H_2O + 2e^- \longrightarrow NO_2^- + 2OH^-, \quad (1)$$

$$Zn^{2+} + 2OH^- \longleftrightarrow Zn(OH)_2\downarrow, \quad (2)$$

$$Al^{3+} + 3OH^- \longleftrightarrow Al(OH)_3\downarrow, \quad (3)$$

$$Zn(OH)_2 \longrightarrow ZnO + H_2O, \quad (4)$$

$$2Al(OH)_3 \longrightarrow Al_2O_3 + 3H_2O. \quad (5)$$

The forms of final products strongly depend on the depositing parameters including the Zn^{2+} ion concentration, applied potential, pH value, temperature, deposition time, distance between electrodes, and active agents. ZnO may be electrodeposited in the form of compact films, hexagonal plates, rods, wires, and even tubes as discussed in literature [28–31]. Supposing the precipitating reaction is controlled at a moderate rate, i.e., when the Zn^{2+} or OH^- ion concentrations in the solutions are very low, one-dimensional hexagonal ZnO nanostructure arrays may be formed by controlling the nucleation and growth process.

In order to choose a suitable applied potential and depositing temperature for growing ZnO NRAs, cyclic voltammetry (CV) was carried out for the aqueous solution of 3 mM $Zn(NO_3)_2$. Figure 1 shows the cyclic voltammogram of the FTO-electrolyte interface recorded upon a first voltammetry scan with the working and counter electrode distance of 2 cm at 20°C and 80°C, respectively. As for the deposition temperature of 80°C (Figure 1(a)), no significant current can be observed at the potential ranging from 0 to -0.8 V, which suggests that no electrochemical reactions occur before the applied potential increases to -0.8 V. A cathodic current starts to increase at about -0.8 V, which can be assigned to the reduction of nitrate ions to nitrite ions. As the applied potential is increased negatively, the cathodic current arises due to the increased rate of the nitrate reduction reaction. Between the applied potentials

from -0.8 V to -2.0 V, there is no obvious other peak current appearing, which proves that no Zn^{2+} ions were reduced to metallic zinc. Kemell et al. [46] had electrodeposited potentiostatically ZnO thin films doped with Al at 80°C from 50 mM $Zn(NO_3)_2$ aqueous solutions containing 1-10 mM $Al(NO_3)_3$. They found that at more negative potentials, the amount of Al decreased and that of Zn increased, which could be attributed to the electrochemically generated hydroxide ions reacting more thermodynamically easily with Al^{3+} ions than with Zn^{2+} ions; when the applied potentials between -1.0 and -1.6 V, the resulted Al concentration in the ZnO films was 2-8 at%.

Generally, a more nonequilibrium growth environment favours for Al^{3+} ions being in situ doped into ZnO lattice via solution chemical routes. Clearly, high Zn^{2+} concentration and applied potential are more favourable for such a nonequilibrium environment. However, in terms of thermodynamics, it may be a contradiction between the growth of one-dimensional single-crystalline ZnO and foreign atoms being doped into ZnO. It may be easy to prepare doped ZnO dense films by electrodeposition method, while this is not necessarily suitable for the growth of one-dimensional crystalline doped ZnO nanostructures. In this work, a relatively high applied potential of -1.5 V, which is aiming at a more nonequilibrium growth environment for Al^{3+} ions entering into ZnO crystal lattice, is chosen for electrochemically growing Al-doped ZnO NRAs. Thereby, the local OH^- concentration near the cathode is relatively high at this applied potential but keeping Zn^{2+} concentration low in the overall solution.

As for the deposition temperature, there appears an anodic peak begins at about -0.9 V when sweeping back the potential for 20°C (Figure 1(b)). It corresponds to the oxidation of the previously deposited metallic Zn, which is consistent with the results of Liang et al. [47]. In comparison, there is no anodic peak detected for 80°C. It may be attributed to the faster consumption of Zn^{2+} ion being precipitated into $Zn(OH)_2$ and thus no more Zn^{2+} ions being reduced into metal zinc at relatively high temperature. In addition, it can be seen that the current density at 80°C is remarkably larger
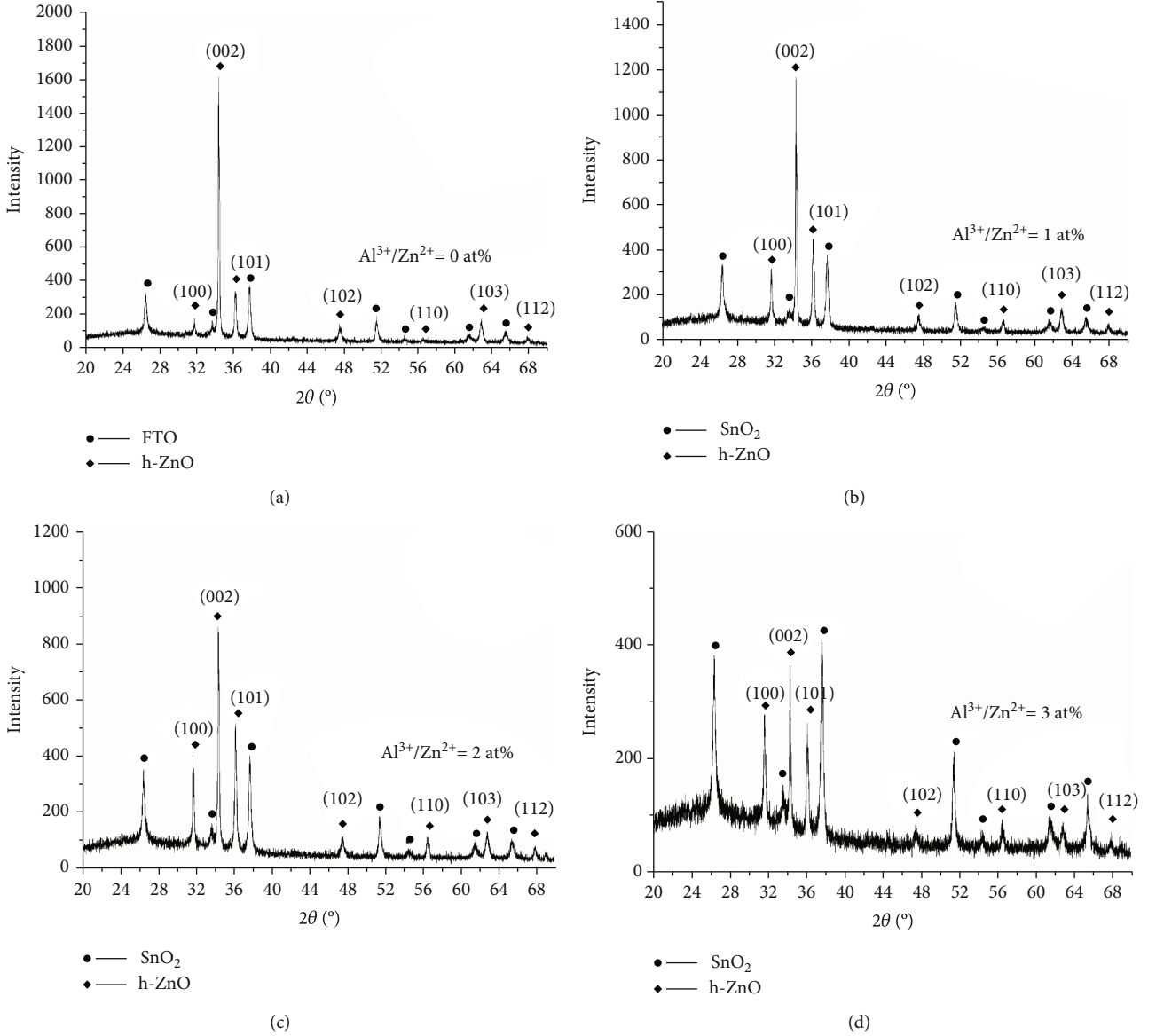
(a)

(b)

(c)

(d)

FIGURE 2: X-ray diffraction patterns of the ZnO samples formed on FTO substrates by electrodeposition method at a constant potential -1.5 V from 3 mM $Zn(NO_3)_2$ aqueous solutions containing $Al(NO_3)_3$ with different Al^{3+}/Zn^{2+} ratio in the bath: (a) 0 at%, (b) 1 at%, (c) 2 at%, and (d) 3 at%, at 80°C for 60 min with a fixed electrode distance of 2 cm.

TABLE 1: Position and intensity of the characteristic peaks of ZnO samples in Figure 2.

Al^{3+}/Zn^{2+} (at%)	$2\theta(002)$	$I(100)$	$I(002)$	$I(101)$	$i(002)$
0	34.4835°	182	1623	344	0.7552
1	34.4579°	316	1169	453	0.6032
2	34.4494°	405	863	518	0.4832
3	34.3984°	280	366	265	0.4018

than that at 20°C at the same applied potentials, which can be assigned to the accelerating of ion migration and reaction rate at higher temperature. On the other hand, the formed $Zn(OH)_2$ can be transformed into ZnO only at elevated temperature.

3.2. Structure and Morphology with Al^{3+}/Zn^{2+} Ratio in the Precursors.
Figure 2 shows X-ray diffraction patterns of the ZnO samples electrodeposited on FTO substrates from 3 mM $Zn(NO_3)_2$ aqueous solutions containing $Al(NO_3)_3$ with different Al^{3+}/Zn^{2+} ratio. It can be seen that all the samples exhibit the characteristic peaks of hexagonal wurtzite ZnO excluding the peaks of polycrystalline tetragonal SnO_2 from the FTO substrates, with no additional peaks corresponding to alumina or other phases. The diffraction peaks of $2\theta = 31.77°$, 34.42°, 36.25°, 47.54°, 56.60°, 62.86°, and 67.96° can be assigned to (100), (002), (101), (102), (110), (103), (112), and (004) planes of hexagonal ZnO. Moreover, the intensity of (002) peak is obviously stronger than that of other peaks, which indicates that the preferred orientation growth along the c-axis perpendicular to the substrates. However, the diffracting peaks of (002) plane become weaker
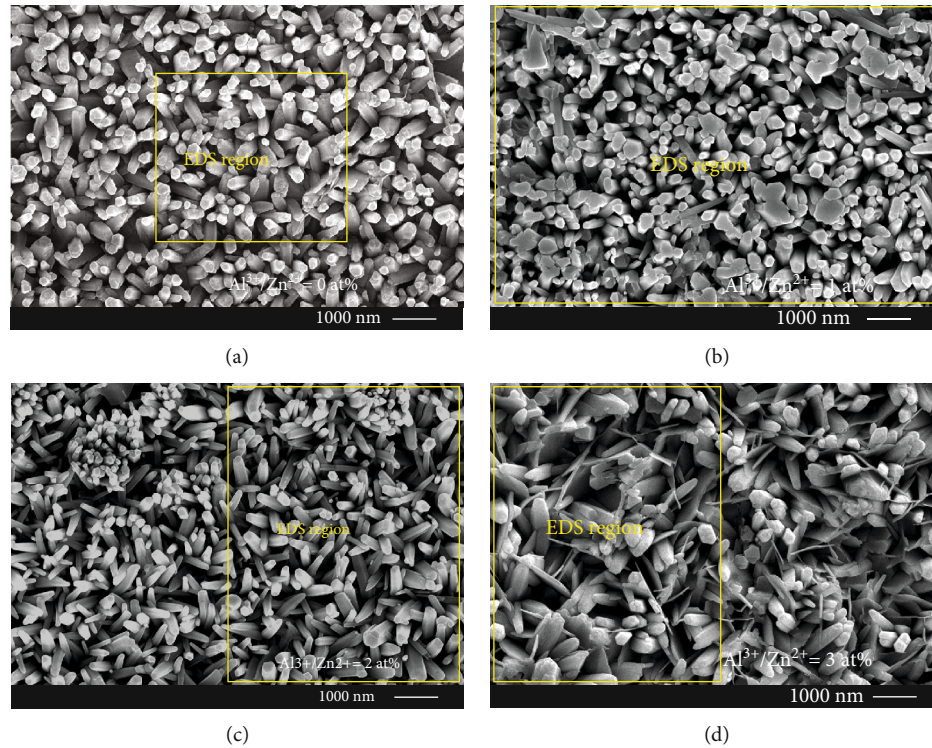
FIGURE 3: SEM images of ZnO films formed on FTO substrates by electrodeposition method at a constant potential -1.5 V from 3 mM $Zn(NO_3)_2$ aqueous solutions containing $Al(NO_3)_3$ with different Al^{3+}/Zn^{2+} ratio in the bath: (a) 0 at%, (b) 1 at%, (c) 2 at%, and (d) 3 at%, at 80°C for 60 min with a fixed electrode distance 2 cm.

with the Al^{3+}/Zn^{2+} ratio increasing, and the pure ZnO sample exhibits the most strongest. As for the sample with an Al^{3+}/Zn^{2+} ratio of 3 at%, it shows no preferred orientation of (002) plane. The (002) preferred orientation growth of ZnO crystals can be also characterized using the relative intensity of (002) plane, which is defined as formula (6) and calculated as shown in Table 1.

$$i(002) = I(002)/[I(100) + I(002) + I(101)], \qquad (6)$$

in which $i(002)$, $I(100)$, $I(002)$, and $I(101)$ are representing the relative intensity of (002) plane and the intensity of (100), (002), and (101) plane, respectively.

It is obvious that the diffracting intensity becomes weaker with the Al^{3+}/Zn^{2+} ratio increasing, which indicates that the existence of Al^{3+} ions in the solutions may affect the depositing and crystallizing process and decrease the crystallinity and preferred orientation growth. It may be attributed to the formation of stress-induced by ion size difference between Zn^{2+} and Al^{3+} ions or the segregation of amorphous alumina in grain boundaries [48]. Besides, it is worth noting that the position of (002) peak shifts to a lower angle with the Al^{3+}/Zn^{2+} ratio increasing, which can be attributed to the lattice strain originating from Al-doping; conversely, it confirms that Al atoms are successfully doped into ZnO lattice.

Figure 3 exhibits morphologies of the same ZnO samples with different Al^{3+}/Zn^{2+} ratio. It can be seen that well-aligned hexagonal ZnO NRAs were grown with the c-axis perpendicular to the substrates except the sample with the Al^{3+}/Zn^{2+}

ratio of 3 at%. There is little difference in the shape, size, and orientation of nanorod arrays for the samples with the Al^{3+}/Zn^{2+} ratios of 0 at% (Figure 3(a)) and 1 at% (Figure 3(b)). The diameter of nanorods is in the range of 80-220 nm. Compared to the former two, the diameter of nanorods for the sample with the Al^{3+}/Zn^{2+} ratio of 2 at% (Figure 3(c)) clearly becomes smaller, which is in the range of 50-120 nm, and its distribution is more uniform. From Figure 3(c) and 3(d), it is more worthy of attention that the deposited Al-doped ZnO films grow into well-aligned hexagonal nanorod arrays with the c-axis perpendicular to the substrates and then transit to a mixture of nanosheets and nanorods.

Figure 4 shows the analysis of X-ray energy dispersive spectra (EDS) and elemental ratio for the samples corresponding to the SEM images in Figure 3, respectively. The Sn, Ca, and Si elements come from the FTO glass substrates. As for the sample with an Al^{3+}/Zn^{2+} ratio of 0 at%, there are no Al atoms detected while existing for other samples, which indicates that Al atoms have been successfully deposited with Zn atoms for the $Zn(NO_3)_2$ aqueous solution containing $Al(NO_3)_3$. It can be seen that the actually resulted Al/Zn ratio in the samples increases with the Al^{3+}/Zn^{2+} ratio in the precursor bath.

Transmission electron microscopy (TEM) was employed to further demonstrate the shape, size, phase, and element composition of the Al-doped ZnO sample with 1 at% Al^{3+}/Zn^{2+} ratio in the precursor, as shown in Figure 5. From the TEM image in Figure 5(a), the diameter and length of the

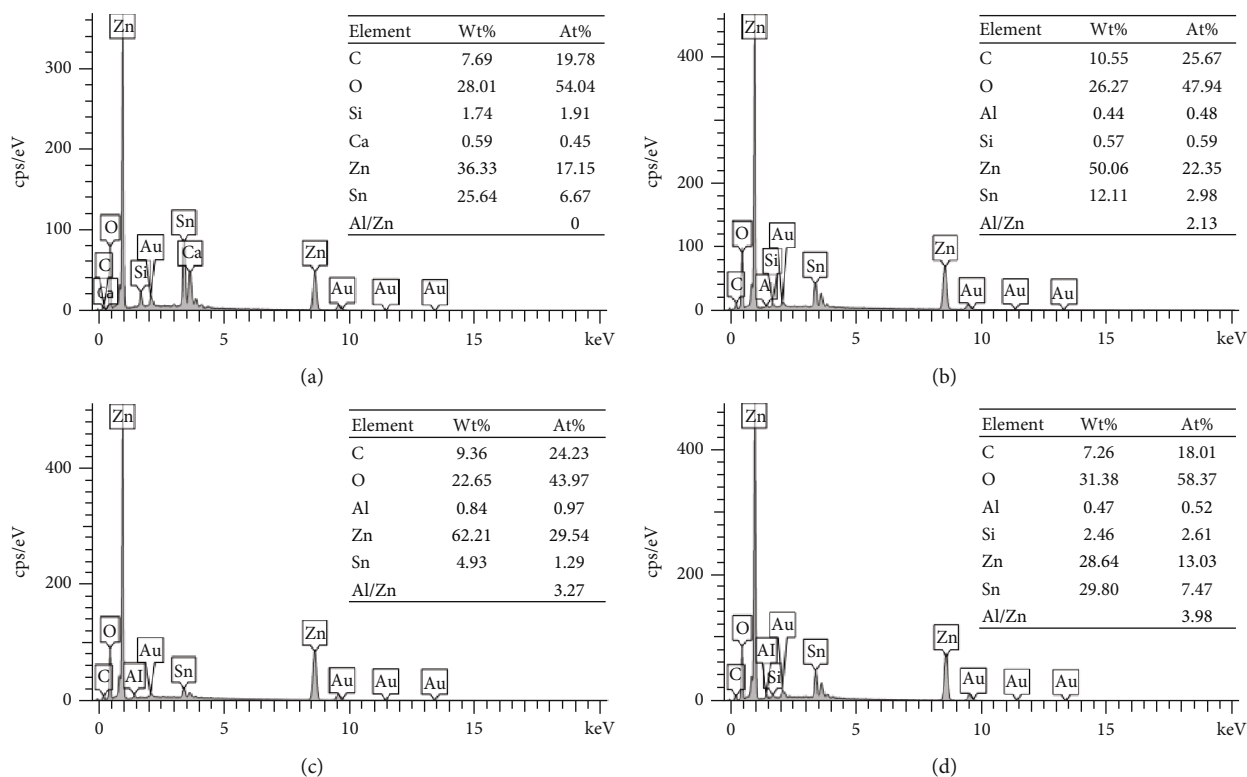| Element	Wt%	At%
C	7.69	19.78
O	28.01	54.04
Si	1.74	1.91
Ca	0.59	0.45
Zn	36.33	17.15
Sn	25.64	6.67
Al/Zn		0

(a)

Element	Wt%	At%
C	10.55	25.67
O	26.27	47.94
Al	0.44	0.48
Si	0.57	0.59
Zn	50.06	22.35
Sn	12.11	2.98
Al/Zn		2.13

(b)

Element	Wt%	At%
C	9.36	24.23
O	22.65	43.97
Al	0.84	0.97
Zn	62.21	29.54
Sn	4.93	1.29
Al/Zn		3.27

(c)

Element	Wt%	At%
C	7.26	18.01
O	31.38	58.37
Al	0.47	0.52
Si	2.46	2.61
Zn	28.64	13.03
Sn	29.80	7.47
Al/Zn		3.98

(d)

FIGURE 4: Energy dispersive analysis of X-ray spectra (EDS) for the ZnO samples corresponding to the SEM images in Figure 3.

(a)

(b)

(c)

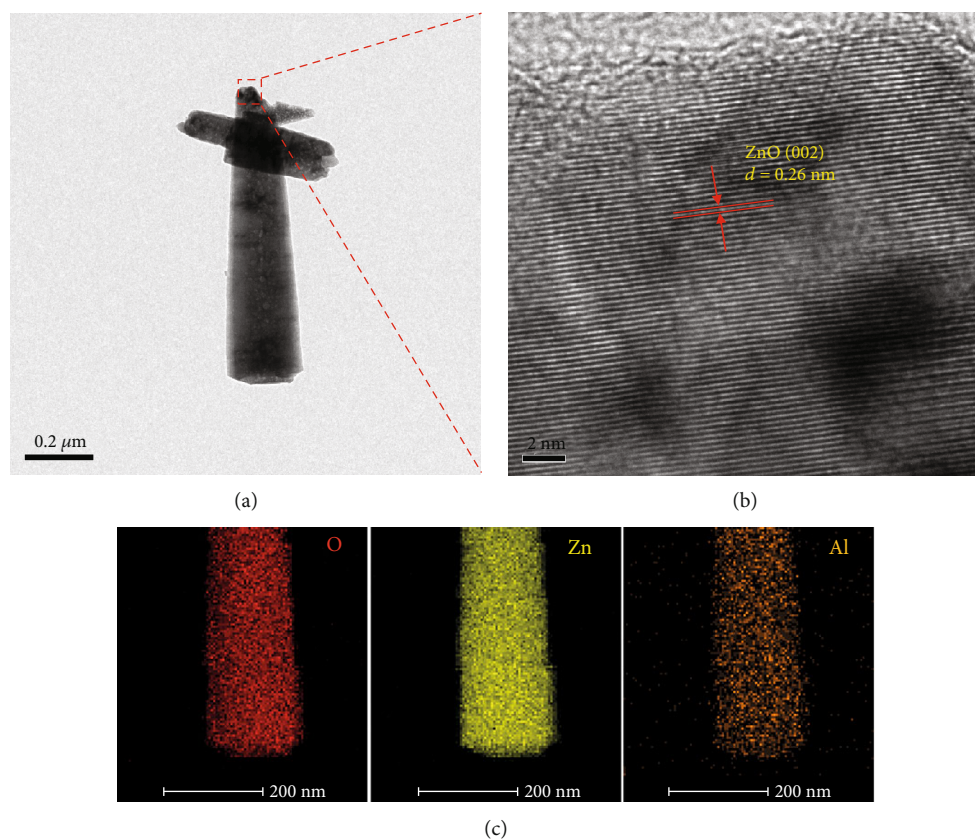FIGURE 5: (a) TEM, (b) HRTEM, and (c) EDS elemental mapping images of the Al-doped ZnO sample with the Al^{3+}/Zn^{2+} ratio of 1 at% in the precursor bath.
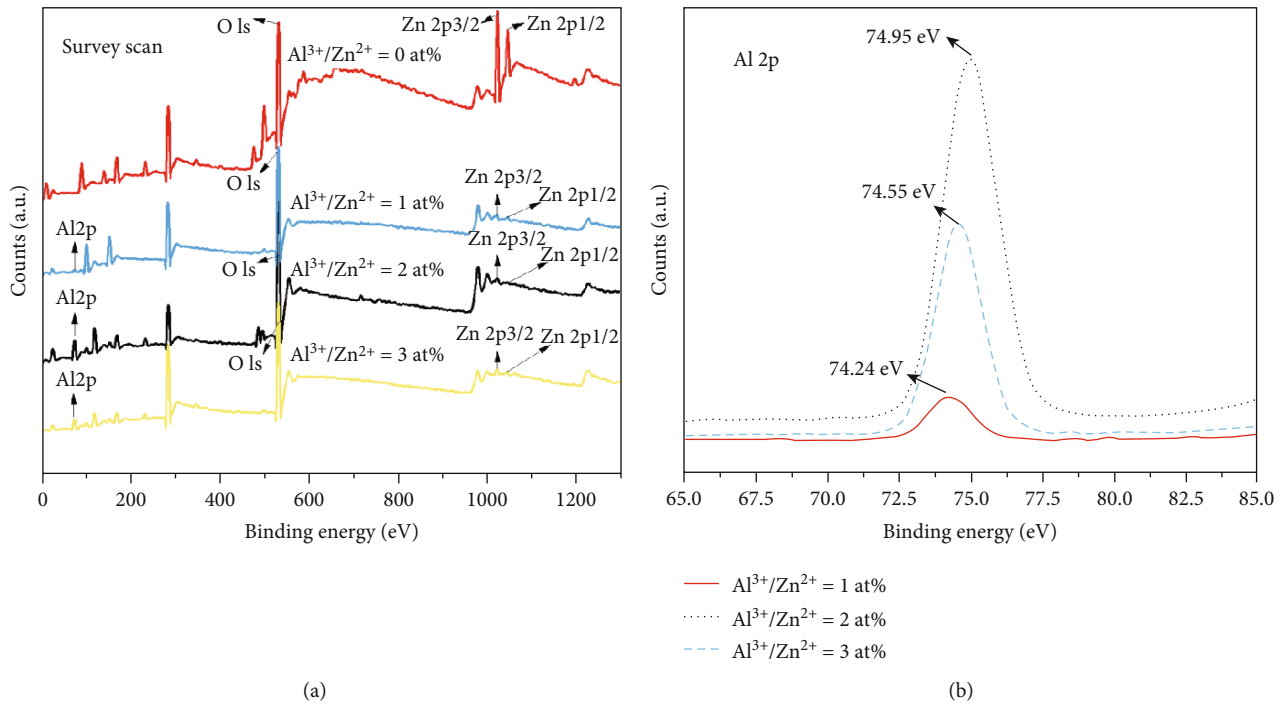
(a)

(b)

FIGURE 6: XPS spectra of (a) survey scan and (b) Al 2p peaks of the ZnO samples with different Al^{3+}/Zn^{2+} ratio in the precursors.
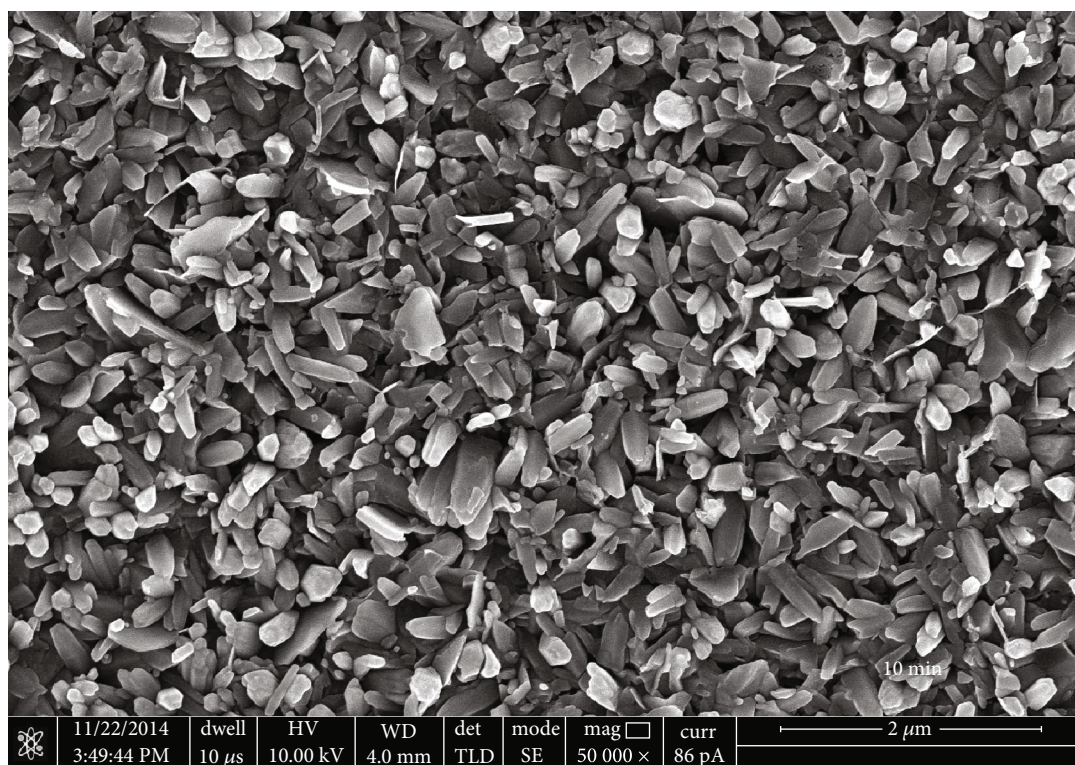
nanorod is 200 nm and 850 nm or so, respectively, which is consistent with those seen from SEM images in Figure 3(b). As zoomed in the square area by high-resolution TEM image of Figure 5(b), the lattice fringes of nanorod are estimated at 0.26 nm, which can be assigned as the (002) plane of hexagonal ZnO, which confirms that the nanorod is hexagonal wurtzite ZnO single crystal. In addition, as seen from the EDS elemental mapping images of the nanorod in Figure 5(c), the Al element is uniformly distributed throughout the nanorod, and the amount of Al element is obviously lower than that of the Zn element.

XPS was adopted to characterize the element composition and chemical bonding state of the pure and Al-doped ZnO samples. Figure 6(a) shows that the full-survey scan spectra exhibit clear peaks of Zn, O, and Al elements in all the Al-doped ZnO samples, while no Al element is detected for the pure ZnO sample, further proving the presence of Al element in the Al-doped ZnO samples. It should be pointed out that the intensity of the Zn element in the pure ZnO sample is greatly stronger than those in the Al-doped ZnO samples. The high-resolution Al $2p$ peaks are shown in Figure 6(b), which locate at 74.24 eV, 74.95 eV, and 74.55 eV for the Al-doped ZnO samples with Al^{3+}/Zn^{2+} ratio of 1, 2, and 3 at% in the precursors, respectively. The binding energy firstly increases with Al^{3+}/Zn^{2+} ratio from 1 at% to 2 at% and then decreases with Al^{3+}/Zn^{2+} ratio rising up to 3 at%, which may be attributed to some amorphous Al_2O_3 phase existing in the Al-doped ZnO sample with 3 at% Al^{3+}/Zn^{2+} ratio.
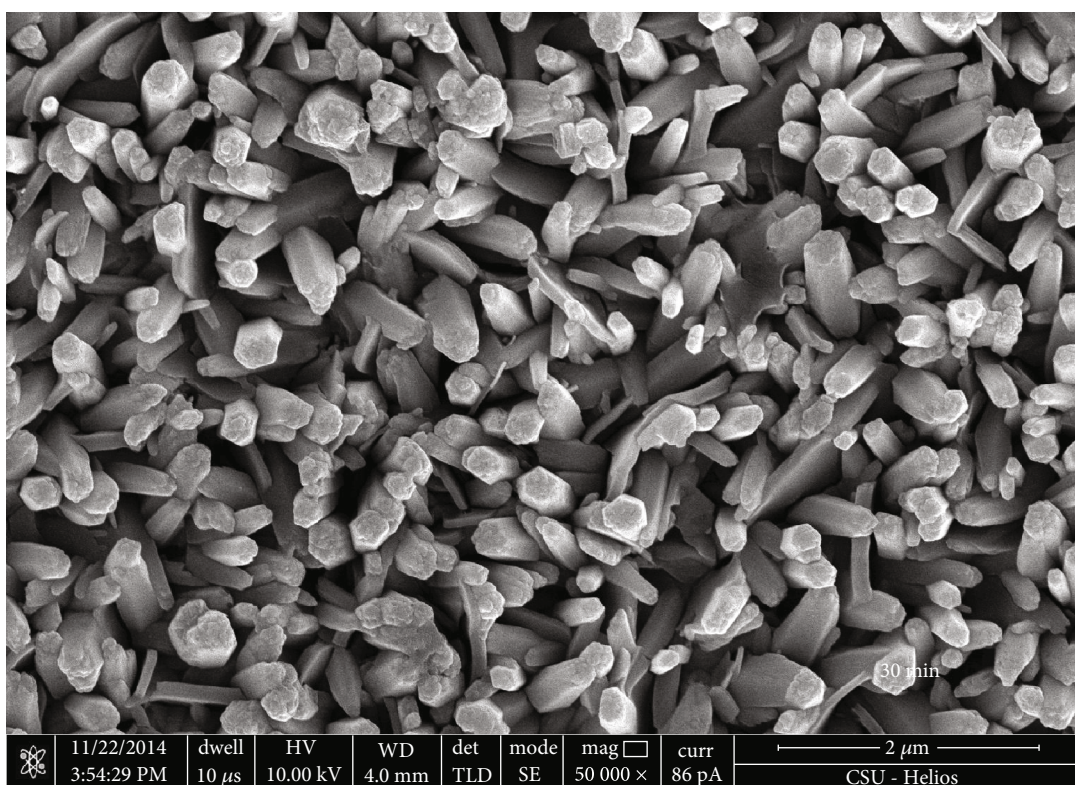
3.3. Morphological Evolution with the Deposition Time. Figure 7 shows the morphological evolution of Al-doped

ZnO electrodeposited from 3 mM $Zn(NO_3)_2$ aqueous solution with Al^{3+}/Zn^{2+} ratio of 1 at% as a function of depositing time. It can be clearly seen that with depositing time increasing (10, 30, 60, and 90 min), the samples gradually grow from small irregular grains into hexagonal crystals. The hexagonal crystals obviously become more perfectly crystalline and larger with the diameter of 200-500 nm corresponding to the depositing time of 90 min.

3.4. Electrical and Optical Properties. The sheet resistance of ZnO samples electrodeposited from 3mM $Zn(NO_3)_2$ aqueous solutions containing $Al(NO_3)_3$ with Al^{3+}/Zn^{2+} ratio of 0, 1, 2, and 3 at% was measured by the four-point-probe method, which was 1856, 167, 95, and 68 Ω/sq, respectively. In our previous work, the sheet resistance of the sample with Al^{3+}/Zn^{2+} ratio of 3.3 at% was 162 Ω/sq [49]. Thus, the sheet resistance of pure and Al-doped ZnO samples as a function of the Al^{3+}/Zn^{2+} ratio in the precursors is shown in Figure 8. It is clearly shown that the electrical conductivity of Al-doped ZnO samples is superior to that of pure ZnO sample, which is increased by almost two orders of magnitude. It also proves that Al atoms are effectively doped into ZnO lattice, which contributes to the enhancement of the electrical conductivity. As for the Al-doped ZnO samples, the conductivity is improved with the Al^{3+}/Zn^{2+} ratio increasing. Of course, the electrical conductivity may be related to many factors including doping effect, crystallinity, crystallite size, and grain boundaries of the samples, as well as oxygen and/or water molecule chemisorbing on the surface. Obviously, the Al-doping effect causing the carrier concentration increasement is the main factor affecting conductivity with very little change in other conditions. It is worth noting
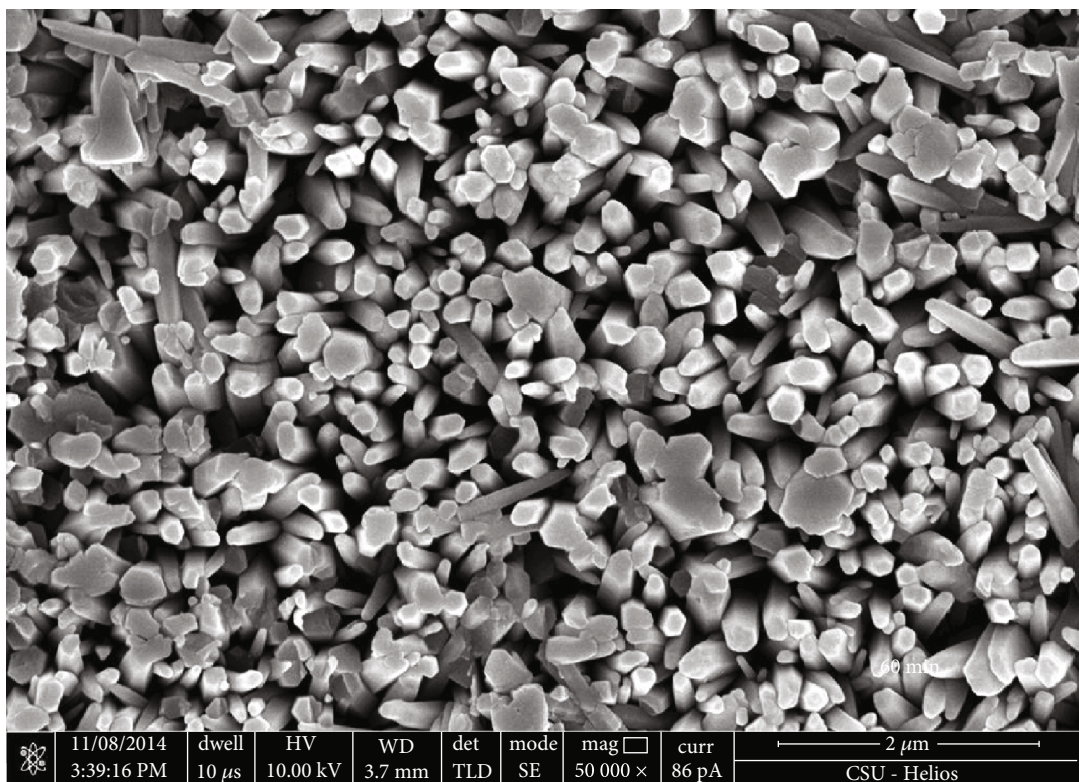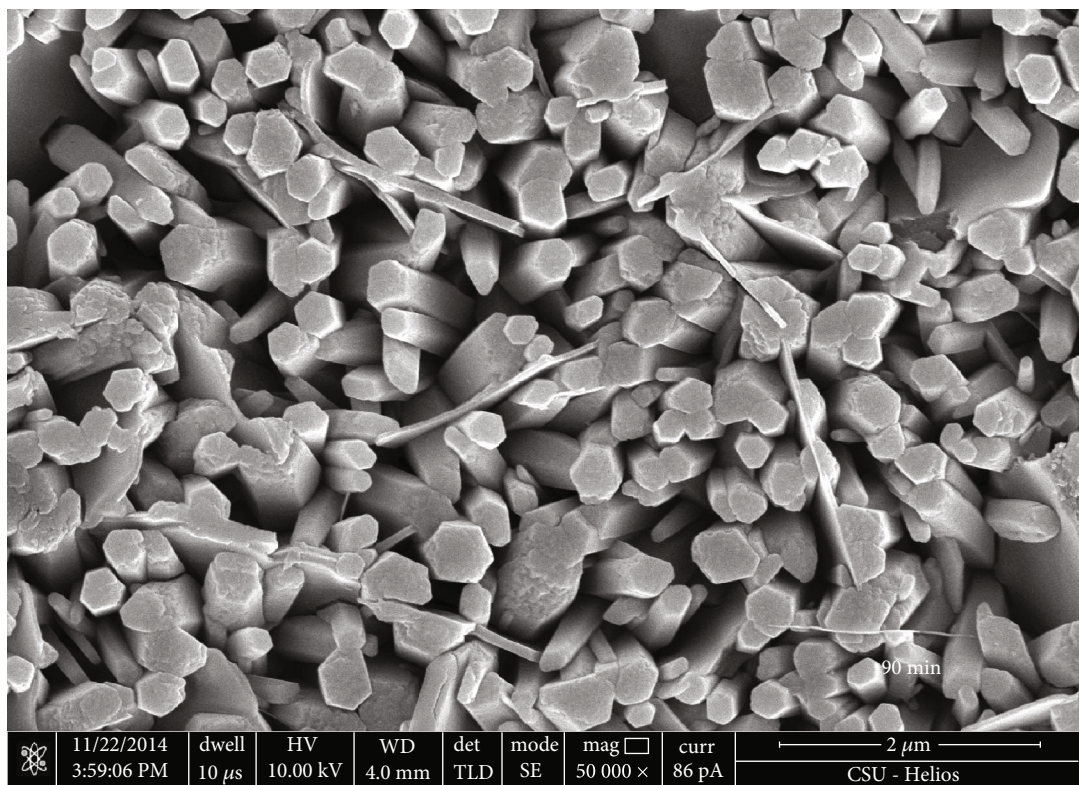
(a)

(b)

Figure 7: Continued.

| 11/08/2014 | dwell | HV | WD | det | mode | mag ☐ | curr | ├──── 2 μm ────┤ |
| 3:39:16 PM | 10 μs | 10.00 kV | 3.7 mm | TLD | SE | 50 000 × | 86 pA | CSU - Helios |

(c)

| 11/22/2014 | dwell | HV | WD | det | mode | mag ☐ | curr | ├──── 2 μm ────┤ |
| 3:59:06 PM | 10 μs | 10.00 kV | 4.0 mm | TLD | SE | 50 000 × | 86 pA | CSU - Helios |

(d)

FIGURE 7: Morphological evolution of Al-doped ZnO NRAs grown by electrodeposition method as a function of deposition time. The deposition parameters: 3 mM $Zn(NO_3)_2$, Al^{3+}/Zn^{2+} ratio 1 at%, 80°C, electrode distance 2 cm, applied potential -1.5 V, deposition time: (a) 10 min, (b) 30 min, (c) 60 min, and (d) 90 min.
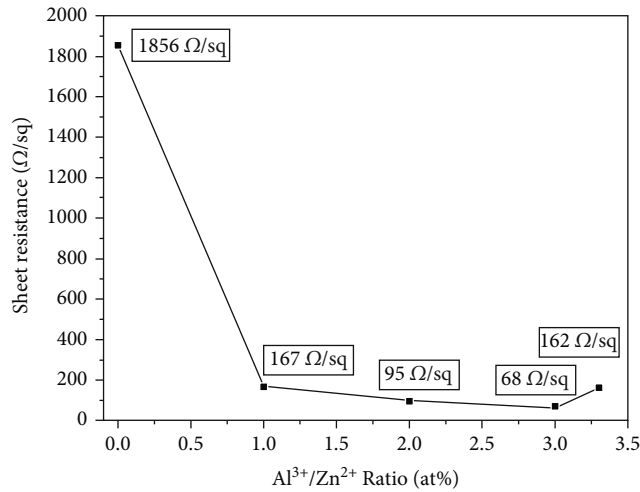
FIGURE 8: Sheet resistance of pure and Al-doped ZnO samples as a function of Al^{3+}/Zn^{2+} ratio in the precursors.
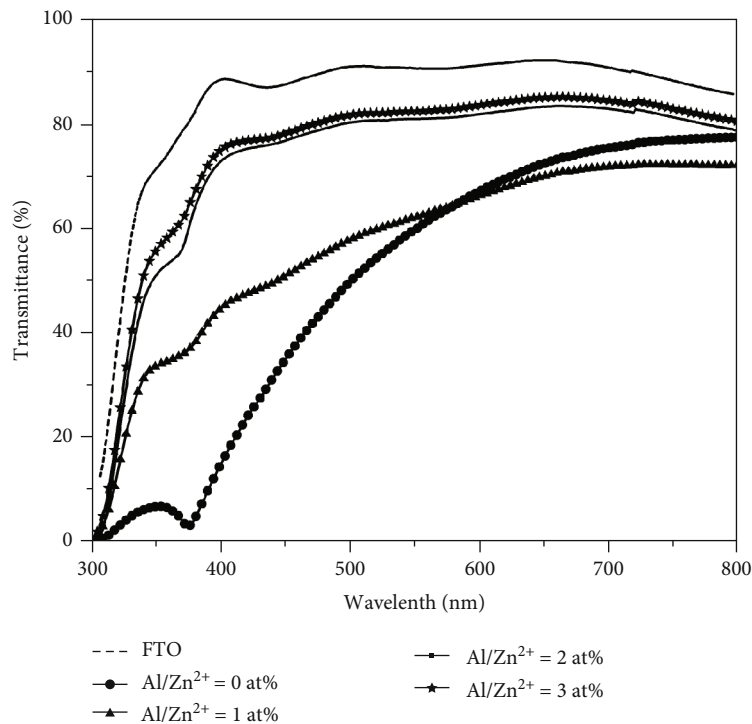

FIGURE 9: Optical transmittance in the visible light wavelength from 300 nm to 800 nm of the FTO glass substrate and the electrodeposited ZnO samples with Al^{3+}/Zn^{2+} ratio of 0, 1, 2, and 3 at% in the precursors and deposition time of 30 min.

whether the deposited Al^{3+} ions existed in the form of Al_2O_3 or are doped into ZnO lattice, or both? It is possible that some amorphous Al_2O_3 phase formed in the grain boundaries when the Al^{3+}/Zn^{2+} ratio increased up to 2 at% although the X-ray results have not detected it in our samples. The growth conditions are vital for the Al^{3+} ion existing state. Many research groups have got similar results, for example, Liang et al. [47] successfully fabricated high crystalline Sb-doped ZnO NRAs with p-type conductivity, and Aragonès et al. [50] electrodeposited Al-doped ZnO films with different doping contents using the electrodeposition

method. However, Zhu and coworkers [51] have investigated the growth of ZnO NRAs by hydrothermal process from aqueous solution composed of 25 mM zinc nitrate and 25 mM hexamethylenetetramine containing different concentration (0, 0.25, 0.5, and 1 mM) aluminium nitrate, and they speculated that Al atoms had not been doped into ZnO lattice. Compared with the electrodeposition process, the hydrothermal growth process may proceed in a relatively more equilibrium environment without applied potential, which may be the cause that Al atoms were unsuccessfully doped into ZnO lattice.
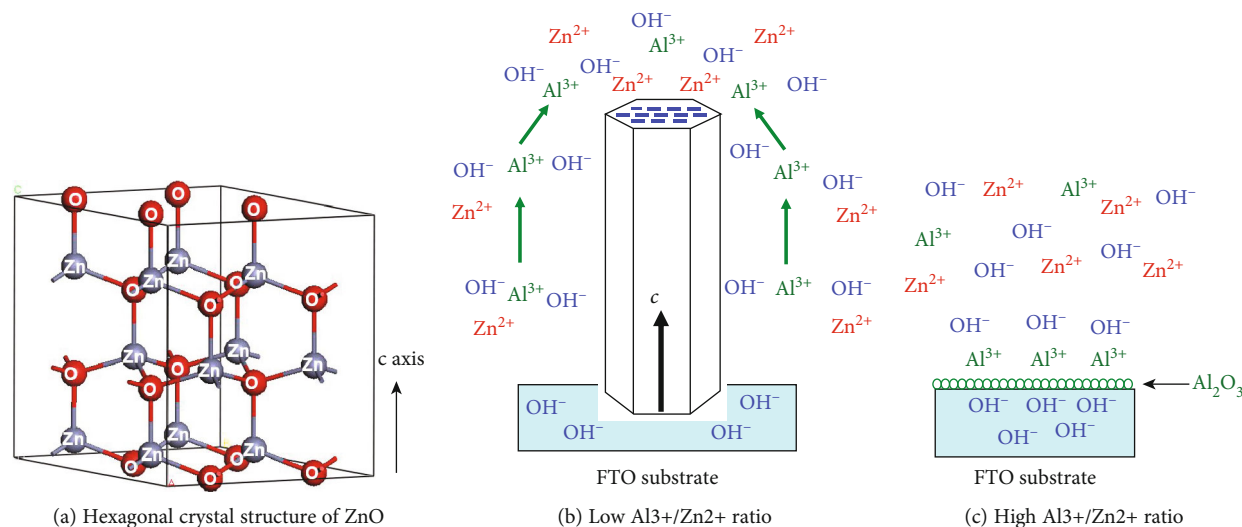
(a) Hexagonal crystal structure of ZnO

(b) Low Al3+/Zn2+ ratio

(c) High Al3+/Zn2+ ratio

FIGURE 10: Schematic diagram of growth principle of ZnO nanorods on FTO substrates by electrodeposition method with different Al^{3+}/Zn^{2+} ratio.

The average transmittance in the visible light wavelength from 400 nm to 700 nm of the FTO glass substrate and the electrodeposited ZnO samples with Al^{3+}/Zn^{2+} ratio of 0, 1, 2, and 3 at% in the precursors and deposition time of 30 min is 91%, 55%, 61%, 81%, and 82%, respectively, as shown in Figure 9. It is obviously seen that the average transmittance of Al-doped ZnO samples is largely higher than that of pure ZnO sample. The average transmittance of 2 at% and 3 at% Al-doped ZnO samples is very close, while with the Al-doping content reducing to 1 at%, the average transmittance of Al-doped ZnO sample decreases to 61%. Considering the light-trapping effect of the nanorod arrays, the relatively low transmittance above 60% of Al-doping ZnO NRAs for transparent electrodes of thin-film solar cells is reasonable. In our other present work, the solar cells based on pure ZnO-NRAs have obtained the best photovoltaic conversion efficiency with a deposition time of 30 min [40, 41], which further confirms the appropriate deposition time for the ZnO NRAs is about 30 min.

3.5. Growth Principle of Electrodepositing Al-Doped ZnO Nanorods. Based on the characteristic and experiment data discussed above, the growth principle of Al-doped ZnO nanorods is proposed. The hexagonal wurtzite ZnO crystals can be considered as a number of alternating planes composed of four-fold coordinated O^{2-} and Zn^{2+} ions stacked alternately along the c-axis in Figure 10(a). The top Zn-terminated (002) plane is positively charged, and the anions from the solution may be absorbed on this polar phase; in the same way, the O-terminated plane is negatively charged and the cations may be absorbed, both resulting in the fast growth of along (002) direction [37, 38]. However, a certain amount of Al^{3+} ions existing in the solution will precipitate with OH^- prior to Zn^{2+}, since the solubility product of $Al(OH)_3$ ($K_{sp} = 4.57 \times 10^{-33}$, 25°C) is remarkably smaller than that of $Zn(OH)_2$ ($K_{sp} = 2.09 \times 10^{-16}$, 25°C) at the same temperature. As illustrated in Figure 10(b), with a relatively

low Al^{3+}/Zn^{2+} ratio in the precursor solution, Zn^{2+} ions with a certain amount of Al^{3+} ions will preferentially absorb on the (002) plane due to the attractive force between positive cations and negative O^{2-} ions, resulting in the preferred growth along the c-axis; with Al^{3+}/Zn^{2+} ratio increasing, more Al^{3+} ions also absorb on other side planes, which will inhibit Zn^{2+} ions from absorbing on these planes, leading to a higher aspect ratio of ZnO nanorods. In contrast, with a high Al^{3+}/Zn^{2+} ratio, more Al^{3+} ions will absorb on the (002) plane and other planes or even on the FTO substrates. However, the product of Al_2O_3 belongs to the insulator, which will prevent the electrochemical reaction from going on [49], as shown in Figure 10(c). Hence, the deposited products will grow into a mixture of nanosheets and nanorods or the electrodeposition process will stop due to the insulating Al_2O_3 layer on the FTO substrates. The result is consistent with the literature [49], which showed that for Al^{3+} concentrations up to 0.3 mM in the electrochemical bath, a top layer of amorphous Al_2O_3 compound was obtained. Therefore, taking into account of desired morphology and phase purity, as well as good electrical conductivity and optical transmittance, the optimal window of Al^{3+}/Zn^{2+} ratio in the precursors is determined at between 1 at% and 2 at% with applied potential of -1.5 V, bath temperature of 80°C, and deposition time of about 30 min.

4. Conclusions

In summary, Al-doped ZnO NRAs have been grown via electrodeposition method from low concentration zinc nitrate aqueous solutions containing a small amount of aluminium nitrate without other auxiliary reagents at a highly negative applied potential. The results showed that Al atoms were successfully doped into ZnO crystal lattice, and the morphologies could be controlled by adjusting the Al^{3+}/Zn^{2+} ratio in the precursors. The deposited Al-doped ZnO films grew into well-aligned hexagonal NRAs with the c-axis perpendicular to the substrates and then transited into a

mixture of nanosheets and nanorods with Al^{3+}/Zn^{2+} ratio increasing or the electrodeposition process will stop due to the insulating Al_2O_3 layer on the FTO substrates. They exhibited good electrical conductivity with sheet resistance of 68-167Ω/square and appropriate visible light transmittance of 61-82%. The optimal window of Al^{3+}/Zn^{2+} ratio in the precursors is determined between 1 at% and 2 at% with applied potential of -1.5V, bath temperature of 80°C, and deposition time of about 30min. The self-assembling method provides a facile and efficient route for obtaining large-area textured transparent conductive Al-doped ZnO NRAs at low cost, which have potential application in transparent electrodes of thin-film solar cells with light trapping.

Data Availability

The CV, XRD, SEM, TEM, XPS, and EDX data used to support the findings of this study are included within the article.

Conflicts of Interest

The authors declare that there is no conflict of interest regarding the publication of this paper.

Acknowledgments

References

[1] Y. F. Hu, Y. L. Chang, P. Fei, R. L. Snyder, and Z. L. Wang, "Designing the electric transport characteristics of ZnO micro-/nanowire devices by coupling piezoelectric and photoexcitation Effects," *ACS Nano*, vol. 4, no. 2, pp. 1234–1240, 2010.

[2] Z. R. Tian, J. A. Voigt, J. Liu et al., "Complex and oriented ZnO nanostructures," *Nature Materials*, vol. 2, no. 12, pp. 821–826, 2003.

[3] L. Gong, J. G. Lu, and Z. Z. Ye, "Transparent conductive Ga-doped ZnO/Cu multilayers prepared on polymer substrates at room temperature," *Solar Energy Materials & Solar Cells*, vol. 95, no. 7, pp. 1826–1830, 2011.

[4] Z. L. Wang and J. H. Song, "Piezoelectric nanogenerators based on zinc oxide nanowire arrays," *Science*, vol. 312, no. 5771, pp. 242–246, 2006.

[5] D. Tamvakos, S. Lepadatu, V. A. Antohe et al., "Piezoelectric properties of template-free electrochemically grown ZnO nanorod arrays," *Applied Surface Science*, vol. 356, pp. 1214–1220, 2015.

[6] P. S. Shewale and Y. S. Yu, "Structural, surface morphological and UV photodetection properties of pulsed laser deposited Mg-doped ZnO nanorods: effect of growth time," *Journal of Alloys and Compounds*, vol. 654, no. 5, pp. 79–86, 2016.

[7] J. J. Li, L. T. Zhang, J. B. Zhu, Y. Liu, and W. C. Hao, "Aligned ZnO:Co nanorod arrays: Electrophoretic deposition fabrication and magnetic manipulation," *Ceramics International*, vol. 41, no. 3, pp. 3456–3460, 2015.

[8] S. Öztürk, A. Kösemen, Z. A. Kösemen, N. Kilinc, Z. Z. Öztürk, and M. Penza, "Electrochemically growth of Pd doped ZnO nanorods on QCM for room temperature VOC sensors," *Sensors and Actuators B: Chemical*, vol. 222, pp. 280–289, 2016.

[9] C. W. Zou, F. Liang, and S. W. Xue, "Synthesis and oxygen vacancy related NO_2 gas sensing properties of ZnO:Co nanorods arrays gown by a hydrothermal method," *Applied Surface Science*, vol. 353, pp. 1061–1069, 2015.

[10] M. Law, L. Greene, J. C. Johnson, R. Saykally, and P. D. Yang, "Nanowire dye-sensitized solar cells," *Nature Materials*, vol. 4, no. 6, pp. 455–459, 2005.

[11] L. Li, T. Y. Zhai, Y. Bando, and D. Golberg, "Recent progress of one-dimensional ZnO nanostructured solar cells," *Nano Energy*, vol. 1, no. 1, pp. 91–106, 2012.

[12] J. J. Wu, W. P. Liao, and M. Yoshimura, "Soft processing of hierarchical oxide nanostructures for dye-sensitized solar cell applications," *Nano Energy*, vol. 2, no. 6, pp. 1354–1372, 2013.

[13] H. Lu, X. Y. Zhai, W. W. Liu, M. Zhang, and M. Guo, "Electrodeposition of hierarchical ZnO nanorod arrays on flexible stainless steel mesh for dye-sensitized solar cell," *Thin Solid Films*, vol. 586, pp. 46–53, 2015.

[14] X. Fang, Y. Li, S. Zhang, L. Bai, N. Y. Yuan, and J. N. Ding, "The dye adsorption optimization of ZnO nanorod-based dye-sensitized solar cells," *Solar Energy*, vol. 105, pp. 14–19, 2014.

[15] Y. M. Sung, F. C. Hsu, and Y. F. Chen, "Improved charge transport in inverted polymer solar cells using surface engineered ZnO-nanorod array as an electron transport layer," *Solar Energy Materials & Solar Cells*, vol. 125, pp. 239–247, 2014.

[16] H. Woo Choi, K. S. Lee, N. David Theodore, and T. L. Alford, "Improved performance of ZnO nanostructured bulk heterojunction organic solar cells with nanowire-density modified by yttrium chloride introduction into solution," *Solar Energy Materials & Solar Cells*, vol. 117, pp. 273–278, 2013.

[17] L. Pan, S. B. Wang, W. B. Mi et al., "Undoped ZnO abundant with metal vacancies," *Nano Energy*, vol. 9, pp. 71–79, 2014.

[18] H. Lu, M. Zhang, and M. Guo, "Controllable electrodeposition of ZnO nanorod arrays on flexible stainless steel mesh substrate for photocatalytic degradation of Rhodamine B," *Applied Surface Science*, vol. 317, pp. 672–681, 2014.

[19] Y. J. Liu, D. Huang, H. X. Liu, T. D. Li, and J. G. Wang, "ZnO tetrakaidecahedrons with co-exposed {001}, {101}, and {100} facets: shape-selective synthesis and enhancing photocatalytic performance," *Crystal Growth & Design*, vol. 19, no. 5, pp. 2758–2764, 2019.

[20] Z. M. Bai, X. Q. Yan, Z. Kang, Y. P. Hu, X. H. Zhang, and Y. Zhang, "Photoelectrochemical performance enhancement of ZnO photoanodes from $ZnIn_2S_4$ nanosheets coating," *Nano Energy*, vol. 14, pp. 392–400, 2015.

[21] R. Lv, T. Wang, F. L. Su, P. Zhang, C. J. Li, and J. L. Gong, "Facile synthesis of ZnO nanopencil arrays for photoelectrochemical water splitting," *Nano Energy*, vol. 7, pp. 143–150, 2014.

[22] Y. J. Liu, H. X. Liu, H. M. Zhou, T. D. Li, and L. N. Zhang, "A Z-scheme mechanism of N-ZnO/g-C_3N_4 for enhanced H_2 evolution and photocatalytic degradation," *Applied Surface Science*, vol. 466, pp. 133–140, 2019.

[23] H. F. Zhai, J. J. Qi, Y. Tan et al., "Construction of 1D-MoS_2 nanorods/$LiNb_3O_8$ heterostructure for enhanced hydrogen evolution," *Applied Materials Today*, vol. 18, article 100536, 2020.

[24] X. Y. Yang, H. X. Liu, T. D. Li et al., "Preparation of flower-like core-shell structure enhances photocatalytic

hydrogen production," *International Journal of Hydrogen Energy*, vol. 45, no. 51, pp. 26967–26978, 2020.

[25] M. Li, X. Qian, A. D. Li, Y. Q. Cao, H. F. Zhai, and D. Wu, "A comparative study of growth and properties of atomic layer deposited transparent conductive oxide of Al doped ZnO films from different Al precursors," *Thin Solid Films*, vol. 646, pp. 126–131, 2018.

[26] H. F. Zhai, B. Y. Xia, and H. S. Park, "Ti-based electrode materials for electrochemical sodium ion storage and removal," *Journal of Materials Chemistry A*, vol. 7, no. 39, pp. 22163–22188, 2019.

[27] Z. N. Jia, X. D. Zhang, Y. Liu, J. Ma, C. C. Liu, and Y. Zhao, "Conductive white back reflector and scatter based on ZnO nanostructure arrays for harvesting solar energy," *Nano Energy*, vol. 1, no. 6, pp. 783–788, 2012.

[28] O. Lupan, V. M. Guérin, I. M. Tiginyanu et al., "Well-aligned arrays of vertically oriented ZnO nanowires electrodeposited on ITO-coated glass and their integration in dye sensitized solar cells," *Journal of Photochemistry and Photobiology A: Chemistry*, vol. 211, no. 1, pp. 65–73, 2010.

[29] T. Pauporte, G. Bataille, L. Joulaud, and F. J. Vermersch, "Well-aligned ZnO nanowire arrays prepared by seed-layer-free electrodeposition and their Cassie-Wenzel transition after hydrophobization," *The Journal of Physical Chemistry*, vol. 114, no. 1, pp. 194–202, 2009.

[30] T. Özdal, R. Taktakoğlu, H. Özdamar, M. Esen, D. K. Takçı, and H. Kavak, "Crystallinity improvement of ZnO nanorods by optimization of low-cost electrodeposition technique," *Thin Solid Films*, vol. 592, pp. 143–149, 2015.

[31] H. Lu, F. Zheng, M. Zhang, and M. Guo, "Effects of preparing conditions on controllable one-step electrodeposition of ZnO nanotube arrays," *Electrochimica Acta*, vol. 132, pp. 370–376, 2014.

[32] N. Kitazawa, M. Aono, and Y. Watanabe, "Growth of vertically aligned one-dimensional ZnO nanowire arrays on sol-gel derived ZnO thin films," *Journal of Physics and Chemistry of Solids*, vol. 75, no. 11, pp. 1194–1200, 2014.

[33] M. Skompska and K. Zarębska, "Electrodeposition of ZnO nanorod arrays on transparent conducting substrates-a review," *Electrochimica Acta*, vol. 127, pp. 467–488, 2014.

[34] A. S. Kamble, B. B. Sinha, K. Chung et al., "Effect of hydroxide anion generating agents on growth and properties of ZnO nanorod arrays," *Electrochimica Acta*, vol. 149, pp. 386–393, 2014.

[35] R.-E. Nowak, M. Vehse, O. Sergeev, K. von Maydell, and C. Agert, "ZnO nanorod arrays as light trapping structures in amorphous silicon thin-film solar cells," *Solar Energy Materials and Solar Cells*, vol. 125, no. 125, pp. 305–309, 2014.

[36] A. Q. Bai, Y. Tang, and J. Chen, "Efficient photon capturing in Cu(In,Ga)Se$_2$ thin film solar cells with ZnO nanorod arrays as an antireflective coating," *Chemical Physics Letters*, vol. 636, pp. 134–140, 2015.

[37] F. Anwar, R. Mahbub, S. S. Satter, and S. M. Ullah, "Effect of different HTM layers and electrical parameters on ZnO nanorod-based lead-free perovskite solar cell for high-efficiency performance," *International Journal of Photoenergy*, vol. 2017, Article ID 9846310, 9 pages, 2017.

[38] P. Wang, J. Zhao, J. Liu et al., "Stabilization of organometal halide perovskite films by SnO$_2$ coating with inactive surface hydroxyl groups on ZnO nanorods," *Journal of Power Sources*, vol. 339, pp. 51–60, 2017.

[39] S. Li, P. Zhang, Y. Wang et al., "Interface engineering of high efficiency perovskite solar cells based on ZnO nanorods using atomic layer deposition," *Nano Research*, vol. 10, no. 3, pp. 1092–1103, 2017.

[40] Z. Y. Peng, Z. Liu, J. L. Chen et al., "Influence of ZnO nano-array interlayer on the charge transfer performance of quantum dot sensitized solar cells," *Electrochimica Acta*, vol. 299, pp. 206–212, 2019.

[41] W. Li, Z. Y. Peng, Z. Sun et al., "Orientation modulation of ZnO nanorods on charge transfer performance enhancement for Sb$_2$S$_3$ quantum dot sensitized solar cells," *Journal of Alloys and Compounds*, vol. 816, article 152628, 2020.

[42] Y. Zhang, G. Zhai, L. Gao et al., "Improving performance of perovskite solar cells based on ZnO nanorods via rod- length control and sulfidation treatment," *Materials Science in Semiconductor Processing*, vol. 117, article 105205, 2020.

[43] D. Commandeur, H. Morrissey, and Q. Chen, "Solar cells with high short circuit currents based on CsPbBr3Perovskite-Modified ZnO nanorod composites," *ACS Applied Nano Materials*, vol. 3, no. 6, pp. 5676–5686, 2020.

[44] P. S. Chandrasekhar, A. Dubey, and Q. Qiao, "High efficiency perovskite solar cells using nitrogen-doped graphene/ZnO nanorod composite as an electron transport layer," *Solar Energy*, vol. 197, pp. 78–83, 2020.

[45] M. R. Khajavi, D. J. Blackwood, G. Cabanero, and R. Tena-Zaera, "New insight into growth mechanism of ZnO nanowires electrodeposited from nitrate-based solutions," *Electrochimica Acta*, vol. 69, pp. 181–189, 2012.

[46] M. Kemell, F. Dartigues, M. Ritala, and M. Leskela, "Electrochemical preparation of In and Al doped ZnO thin films for CuInSe$_2$ solar cells," *Thin Solid Films*, vol. 434, no. 1-2, pp. 20–23, 2003.

[47] J. K. Liang, H. L. Su, C. L. Kuo et al., "Structural, optical and electrical properties of electrodeposited Sb-doped ZnO nanorod arrays," *Electrochimica Acta*, vol. 125, pp. 124–132, 2014.

[48] H. M. Zhou, D. Q. Yi, Z. M. Yu, L. R. Xiao, and J. Li, "Preparation of aluminum doped zinc oxide films and the study of their microstructure, electrical and optical properties," *Thin Solid Films*, vol. 515, no. 17, pp. 6909–6914, 2007.

[49] J. L. Chen, J. Chen, D. Chen et al., "Electrochemical deposition of Al-doped ZnO transparent conducting nanowire arrays for thin-film solar cell electrodes," *Materials Letters*, vol. 117, pp. 162–164, 2014.

[50] A. C. Aragonès, A. Palacios-Padrós, F. Caballero-Briones, and F. Sanz, "Study and improvement of aluminium doped ZnO thin films: limits and advantages," *Electrochimica Acta*, vol. 109, pp. 117–124, 2013.

[51] S. B. Zhu, X. Tian, L. M. Shan et al., "Effect of Al^{3+} on the growth of ZnO nanograss film and its application in dye-sensitized solar cells," *Ceramics International*, vol. 39, no. 8, pp. 9637–9644, 2013.